International Journal of Nanomedicine

Dovepress
open access to scientific and medical research

Open Access Full Text Article

ORIGINAL RESEARCH

Self-Assembly Nanoparticles for Overcoming Multidrug Resistance and Imaging-Guided Chemo-Photothermal Synergistic Cancer Therapy

This article was published in the following Dove Press journal:
International Journal of Nanomedicine

Haiyan Gao[1,2]
Yan Bai[1,2]
Lijuan Chen[1,2]
Georges Ei Fakhri[3]
Meiyun Wang[1,2]

[1]Henan Provincial People's Hospital & Zhengzhou University People's Hospital, Zhengzhou 450003, People's Republic of China; [2]Henan Key Laboratory of Neurological Imaging, Zhengzhou University, Zhengzhou 450003, People's Republic of China; [3]Gordon Center for Medical Imaging, Radiology, Massachusettes General Hospital, Harvard Medical School, Boston, MA 02114, USA

Background and Purpose: The development of multiple drug resistance (MDR) to chemotherapy and single modal therapy remains unsatisfied for the eradication of tumor, which are major obstacles in cancer therapy. This novel system with excellent characteristics for inhibition of P-glycoprotein (P-gp), and for near-infrared fluorescence (NIRF) imaging-guided chemo-photothermal therapy (PTT), has been identified as a promising way to MDR and achieve synergistic cancer therapy.

Methods: In this study, we successfully synthesized a multifunctional theranostic system, which was developed through FDA-approved self-assembling drugs, which contain anticancer drug doxorubicin (Dox), imaging and high photothermal conversion drug indocyanine green (ICG) and P-gp regulator TPGS (the system named T/Dox-ICG). We studied the characterization of T/Dox-ICG NPs, including the TEM, SEM, DLS, UV-vis-NIR, zeta potential, CLSM, in vitro FL imaging, in vitro photothermal effect, in vitro Dox and ICG release. We used CLSM to verify the location of intracellular distribution of Dox in SCG 7901/VCR cells, Western blot was performed to demonstrate the TPGS-mediated inhibition of P-gp. And, the cytotoxicity of materials against SCG 7901/VCR cells was studied by the MTT assay.

Results: The TEM showed the T/Dox-ICG NPs had good monodispersity with diameters of 19.03 nm, Dox and ICG could be released constantly from T/Dox-ICG NPs in vitro. In vitro cell experiments demonstrated higher Dox accumulation and retention in the nucleus. Western blot showed TPGS could obviously inhibit the expression of P-gp. In vitro cytotoxicity assay showed more significant cytotoxicity on MDR cells (SCG 7901/VCR) with only 8.75% of cells surviving.

Conclusion: MDR cancer therapy indicates that it may be important to develop a safer system that can simultaneously inhibit the drug transporters and monitor the delivery of chemotherapeutic agents, and combination therapy have raised widespread concern on tumor treatment.

Keywords: multiple drug resistance, self-assembling, synergistic cancer therapy, imaging-guided therapy

Introduction

Cancers have currently become a severe health threat all over the world.[1] There has been tremendous progress in the treatment of cancer including chemotherapy, radiation therapy, immunotherapy, photodynamic therapy (PDT) and photothermal therapy. Chemotherapy remains the most common therapeutic modality due to its high efficiency.[2] PTT is also a highly effective intervention to ablate tumor tissues in a noninvasive and harmless manner.[3] However, these types of single modal therapy have a limited effectiveness of completely tumor eradication without any recurrence.[4] Thus, combination therapy with different therapeutic agents and anticancer mechanisms

Correspondence: Meiyun Wang
Email mywang@ha.edu.cn

submit your manuscript | www.dovepress.com
DovePress
http://doi.org/10.2147/IJN.S232449

has been developed as a more preferable therapeutic modality. Taking advantage of each modality, combination therapy may suppress tumor growth cooperatively.[5–9] And "chemotherapy + PTT" has been explored as a promising modality to augment tumor treatment.[10–12]

As we all know, chemotherapy suffer from major limitations. Its toxic side effects damage normal tissues, and another challenge is that chemotherapeutic agents could induce MDR in tumors after prolonged treatments. One well investigated mechanism of MDR is the overexpression of efflux pumps on the cell surfaces, such as, the ABC-transporter family P-gp. P-gp, which is also called drug pump, is expressed in various of tumors. It transports drugs out of the cells,[11] hence reducing the intracellular accumulation of chemotherapeutic agents. Several inhibitors and modulators of P-gp have been developed to co-delivery with anticancer drugs to achieve the aim of reversing MDR, but their use have been limited to high toxicity and unfavorable pharmacokinetic interactions.[13,14] Recently, it was reported that the combination of chemotherapeutics and siRNA targeting MDR genes loaded in nanomaterials can overcome MDR and kill the cancer cells.[15–19] However, the delivery of drug/gene into tumors strongly relies on the sophisticated design of drug delivery system (DDS), and drug/gene is required to be released in a controlled manner. On the other hand, the biosafety of DDS also remains a concern. Therefore, there is an urgent need for a drug delivery method that is safe, can overcome multidrug resistance, and has an optimized antitumor therapeutic efficacy.

To date, multifunctional nanoplatforms were designed for both diagnostic and therapeutic features, which have attracted great interests. Nanoparticle designed for diagnostic purposes can monitor the delivery of chemotherapeutic agents, thus it can guide the cancer therapy. Typical examples include NIRF imaging, photoacoustic (PA) imaging, ultrasound (US) imaging, magnetic resonance (MR) imaging and positron emission tomography (PET) imaging.[20–24] Although traditional delivery formulations combined therapeutic agents and imaging agents into a nanoplatform, its potential toxicity, overly complicated design, and poor drug loading capacity of nanocarriers make this type of treatment far too impractical for clinical application. To solve this issue, nanotheranostics that are achieved directly from small molecules without any carrier have attracted great attention.[25–28] Self-delivered drug is a safer method, and it could also achieve high drug loading as carriers are no longer necessary. Moreover, it is relatively easy to mass produce.[29–34] Scientists have already studied nanodrug self-delivery systems formed by two or more different drugs for combination cancer therapy.[27] However, few reports have been reported about nano-drug previously designed by photothermal agent and chemotherapeutic drug directly for imaging-guided combination therapy, and simultaneously overcome multidrug resistance of tumors which are not sensitive to chemotherapy.

Dox, an anthracycline that can interact with DNA, is highly effective used to treat a wide variety of cancers.[8,35,36] ICG, the common NIR organic dye for noninvasive bioimaging and drugs for cancer PTT.[37] Herein, we consider that Dox and ICG can self-assemble to form nanoparticles due to electrostatic, π–π stacking, or hydrophobic interactions. In addition, TPGS is a water-soluble macromolecule derived from natural vitamin E, it has been used as a safe carrier for drug delivery and widely used in nanomedicine.[38–40] Moreover, TPGS is an excellent surfactant, a good candidate that serves as an emulsifier, drug solubilizer and stabilizer. Nanoparticles with TPGS can extend blood circulation time.[41,42] Furthermore, TPGS could serve as an inhibitor of P-gp to combat MDR. The P-gp inhibition mechanisms may be considered to include down-regulation expression of P-gp, inhibition of P-gp ATPase and mitochondria membrane potential decrease.[43–45] In this work, we developed a theranostic NP that is self-assembled by FDA-approved agents, allowing for fluorescence (FL) imaging-guided chemo-PTT cancer therapy and the reversal of MDR. TPGS are used for a surfactant for NPs. It improves the dispersion of drugs in water, increases cellular uptake of drugs and restores sensitivity to chemotherapeutic drugs in drug-resistant cells. A large number of Dox and ICG could be delivered themselves into tumor sites, to kill tumor cells synergistically. Thus, the NP system is a promising candidate for imaging-guided drug-resistant tumor ablation (Figure 1).

Materials and Methods

Materials

Doxorubicin was obtained from Dalian Meilun Biotech Co., Ltd (Dalian, China). D-α-tocopheryl polyethylene glycol 1000 succinate (TPGS) was purchased from Ai Keda Chemical Technology Co., Ltd (Chengdu, China). 3-(4,5-dimethyl-2-thiazolyl)-2,5-diphenyl-2-H-tetrazolium bromide (MTT) was obtained from Sigma Chemical Corporation (USA). Indocyanine green was obtained from Meilunbio (China).

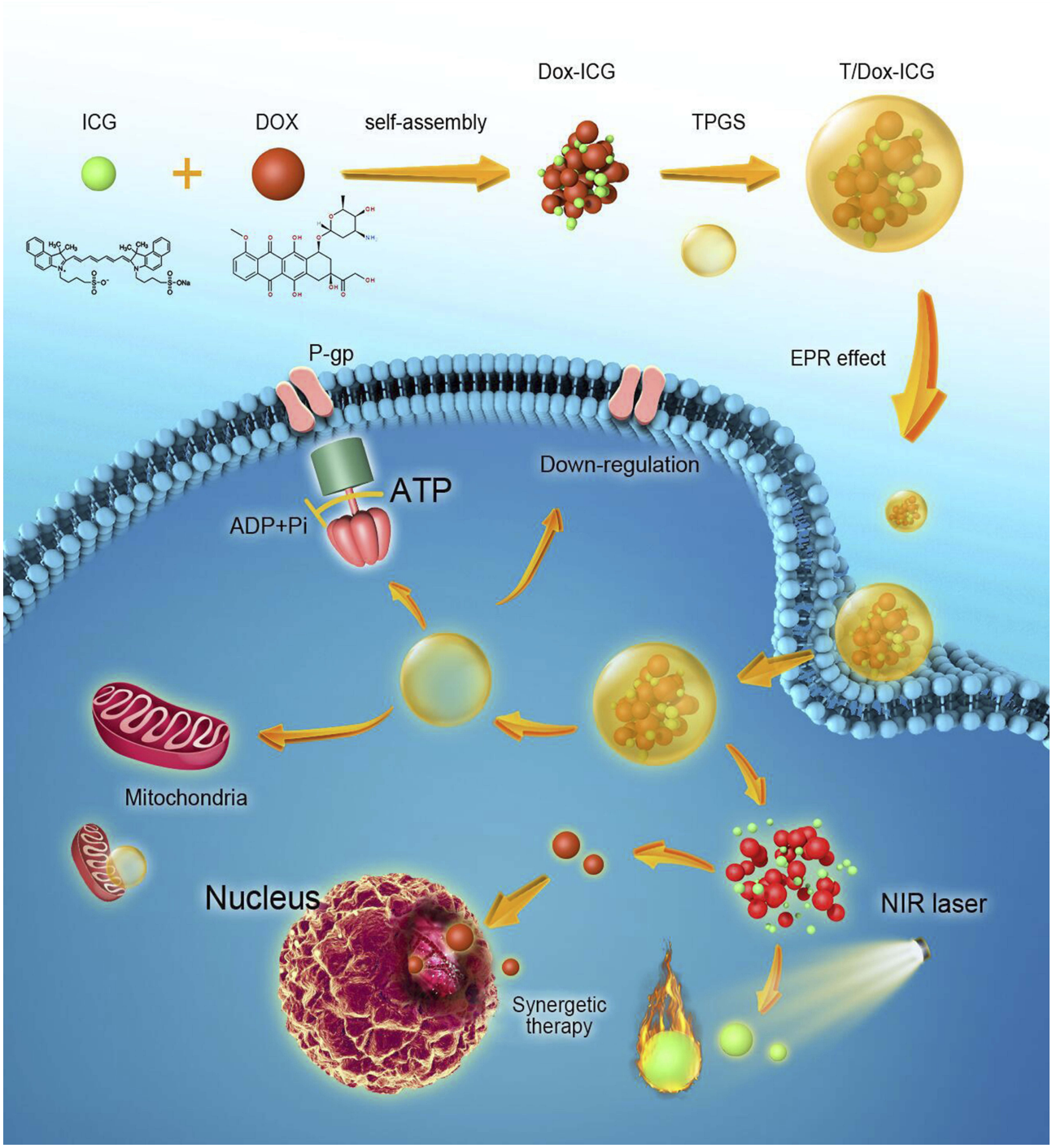

Figure 1 A multifunctional theranostic system, which was developed through FDA-approved self-assembling drugs, which contain anticancer drug doxorubicin (Dox), imaging and high photothermal conversion drug indocyanine green (ICG) and P-gp regulator TPGS. This novel system is a promising candidate for imaging-guided drug-resistant tumor ablation.

All other chemicals were of reagent grade. Water was purified with a Milli–Q Plus 185 water purification system (Millipore, Bedford, MA). Multidrug-resistant gastric cancer cell line SCG7901 was gift by the Fourth Military Medical University Chinese Academy of Sciences, and the cells were purchased commercially by them. DAPI, Calcein-AM, and propidium iodide (PI) were obtained from Invitrogen (USA). Cell lysates (RIPA) and Protease inhibitor (PMSF) were bought from Sigma Chemical Corporation (USA). P-gp antibody was obtained from Abcam. HRP-labeled goat antimouse IgG secondary antibody was got from Sunshine bio (China), and ECL kit was obtained from Promega (China).

Preparation of Dox-ICG and T/Dox-ICG NPs

First, Dox-ICG NPs were prepared by self-assembly technique. In brief, Dox and ICG were dissolved in 20 mL deionized water with the mass ratio of 1:1 and 1:2. Then, the mixture solution was stirred at room temperature for 12 h. After that, the product was centrifuged at 7, 000 g for 10 min, then washed by deionized water several times to remove excess Dox and ICG. After determining the appropriate ratio of two drugs, TPGS was added to Dox-ICG solution and stirred for 2 h at room temperature (mass ratio = 1:1:1). Next, an Amicon Ultra-15 centrifugal filter (MWCO 10KD, USA) was used to wash the resulting solution for three times to remove TPGS.

Characterization of Dox-ICG and T/Dox-ICG NPs

The morphology of the Dox-ICG and T/Dox-ICG NPs was characterized by transmission electron microscopy (TEM, JEOL, Japan). The morphology of T/Dox-ICG NPs was also measured by scanning electron microscope (SEM, JEOL JSM-5900, Japan). The size, size distribution, and zeta potential of these nanoparticles were analyzed by an SZ-100 Nano Particle analyzer (Horiba Scientific). Ultraviolet−visible-near-infrared (UV−vis-NIR) absorbance spectra were recorded with a microplate reader (SH-1000 Lab, Japan). The Dox and ICG encapsulation efficiency were then studied by UV−vis spectrophotometer at 480 nm and 780 nm, respectively. The obtained T/Dox-ICG NPs were also observed by CLSM (Olympus, Germany). The fluorescence spectra were performed on an LS-55 luminescence spectrometer (PerkinElmer, Inc., USA; ex: 740 nm). The in vitro FL imaging and FL signals intensity of particles were obtained at 780 nm with fluorescence intensity with Carestream FX PRO fluorescence imaging system. The photothermal capacity of samples was evaluated using an 808 nm NIR laser. The drug encapsulation efficiency and drug-loading content are acquired through the following formula:

drug encapsulation efficiency (%) = (weight of loaded drug) / (weight of initially added drug) × 100%;

drug-loading content (%) = (weight of loaded drug) / (total weight of NPs) × 100%.

In vitro Drug Release

In vitro release profiles of Dox and ICG from T/Dox-ICG NPs were evaluated as follows: 2 mL solution was added to a dialysis bag (MWCO 10, 000 Da), and incubated in PBS (pH 5.5 and 7.4) at 37°C in a 50 mL centrifuge tube under horizontal shaking at 300 rpm. Then, 1 mL of the release solution was taken out and replaced with new equal volume of PBS at selected time point. The released Dox and ICG content were detected by UV−vis spectrometry at 480 nm and 780 nm, respectively. The tests were repeated three times.

Cell Culture

Multidrug-resistant SCG 7901/VCR cells were incubated in RPMI-1640 medium supplemented with 10% FBS and 1% antibiotics at 37°C with 5% CO_2. During the cell culture, 1 mg/mL vincristine was added to the medium to maintain the resistant phenotype.

In vitro Cellular Uptake and Intracellular Distribution of Dox

The cellular uptake of Dox-ICG, T/Dox-ICG NPs and intracellular Dox accumulation and retention was performed on the confocal fluorescence microscope (Nikon C2). SCG 7901/VCR cells were seeded onto cell culture dishes, after 24 hrs incubation, the cells were treated with Dox-ICG, T/Dox-ICG NPs (Dox concentration 10 μg/mL). After incubation for 12 and 24 h, the cells were washed with cold PBS for three times, and fixed by 4% paraformaldehyde for 10 min, washed with PBS thrice again, and then stained with DAPI for 10 min and washed. The dishes were further imaged under the CLSM.

Western-Blot Assay

The P-gp level was tested by western-blot. Cells were seeded in 10 cm plates, which containing $5*10^6$/plate, the cells were exposed to Dox-ICG and T/Dox-ICG treatment. After 24 hrs incubation, the cells with all groups were collected and washed, then lysed in RIPA buffer (50 mM Tris–HCl pH 7.5, 150 mM NaCl, 1% NP-40, 0.1% SDS, 0.5% deoxycholate, 1 mM EDTA) containing 1mM phenylmethylsulfonyl fluoride on the ice for 30 min, and got the cell lysates. Using bicinchoninic acid (BCA) method to measure total protein, protein was loaded SDS-PAGE equally, after 120v/2h, the gel was transferred onto PVDF membrane, the membrane was blocked with BSA 1 hrs and washed with twain 20 three times, then was incubated with mouse monoclonal IgG1 of P-gp at 40°C overnight. After that, the membrane was first washed three to five times, and incubated with HRP-labeled goat anti-mouse IgG secondary antibody at room temperature for

1 h. After washed, added color liquid, and exposed to signals were detected with the ECL kit, actin was used as an internal control.

In vitro Cytotoxicity Assay

SCG 7901/VCR cells were cultured onto 96-well plates containing 100 μL medium, to obtain a concentration of 10,000 cells per well. After overnight incubation, Dox, free ICG, Dox-ICG and T/Dox-ICG NPs were added to treat cells for 12 h at 37°C under 5% CO_2 in the dark. Next, the cells were washed with fresh medium, and then exposed to an 808 nm laser at 1 W/cm^2 for 5 min, followed by a further incubation of 37°C under 5% CO_2 for 6 h. After an extra 6 h of incubation in the dark, the cell viability was evaluated by the MTT assay. For the T/Dox-ICG NPs with 808 nm laser group, the cells were seeded onto a 6-well plate and then incubated for 24 h. and treated with T/Dox-ICG NPs 12-hr incubation in the dark. The cells were replaced with fresh culture medium, irradiated with or without an NIR laser for 5 min. After further incubation for 12 h, the cells were washed with PBS three times and stained with Calcein-AM and PI.

Results and Discussions

Preparation and Characterization of Dox-ICG and T/Dox-ICG NPs

To prepare the self-delivered system with three agents for chemotherapy-resistant tumor imaging and therapy. We first explored the appropriate proportion of Dox and ICG. Dox and ICG were designed based on electrostatic interactions, π–π stacking, or hydrophobic interactions. Dox and ICG were mixed in a ratio of 1:1 and 1:2, we noted that the size of Dox-ICG NPs can be adjusted by altering the mass ratio of Dox to ICG. The transmission electron microscopy (TEM) revealed that the morphology and dispersion of ICG-Dox NPs were relatively uniform with a mass ratio of 1:1 (Figure 2A and B), and dynamic light scattering (DLS) data also suggested the size of Dox-ICG NPs can be adjusted by altering the mass ratio of Dox to ICG, and we found its size distributions displayed a spacious feature, which reflects the uneven morphology of the particle (Figure 3A). Ultraviolet-visible-near-infrared (UV-vis-NIR) absorption of Dox-ICG was shown in Figure 3B. Surprisingly, as the ratio of Dox to ICG increased, its absorption value decreased accordingly, which might be

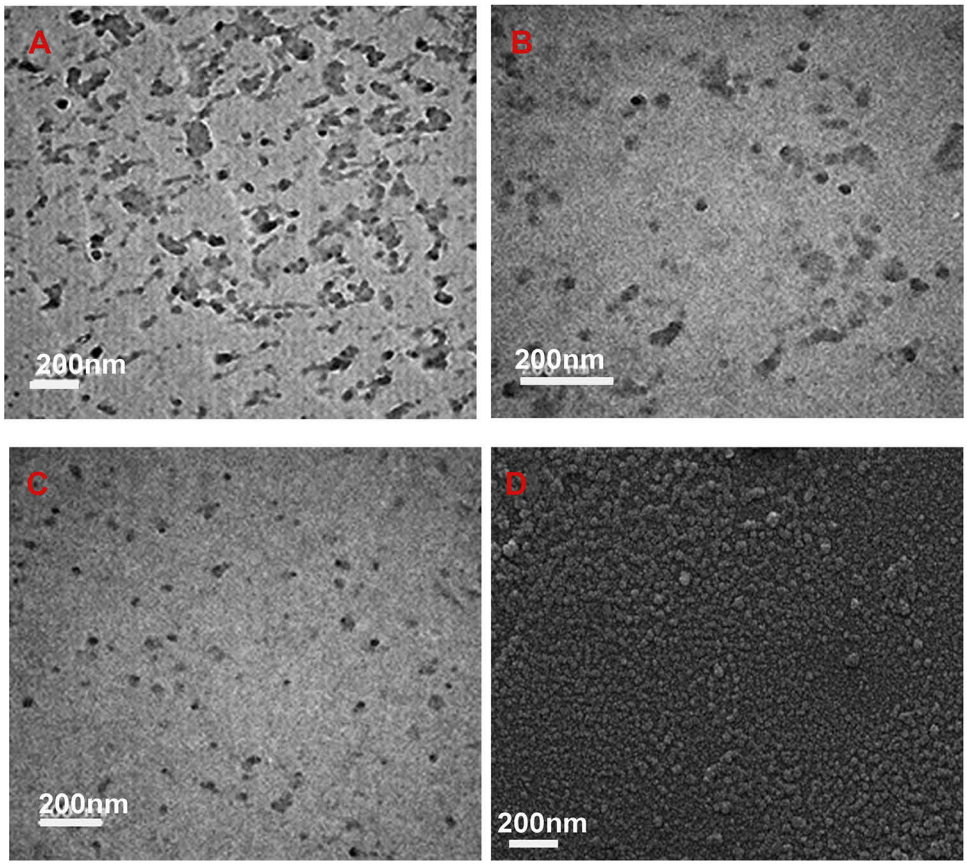

Figure 2 (**A**) TEM images Dox-ICG (1:2), (**B**) TEM images Dox-ICG (1:1) and (**C**) TEM images T/Dox-ICG NPs (1:1:1). (**D**) SEM images of T/Dox-ICG NPs.

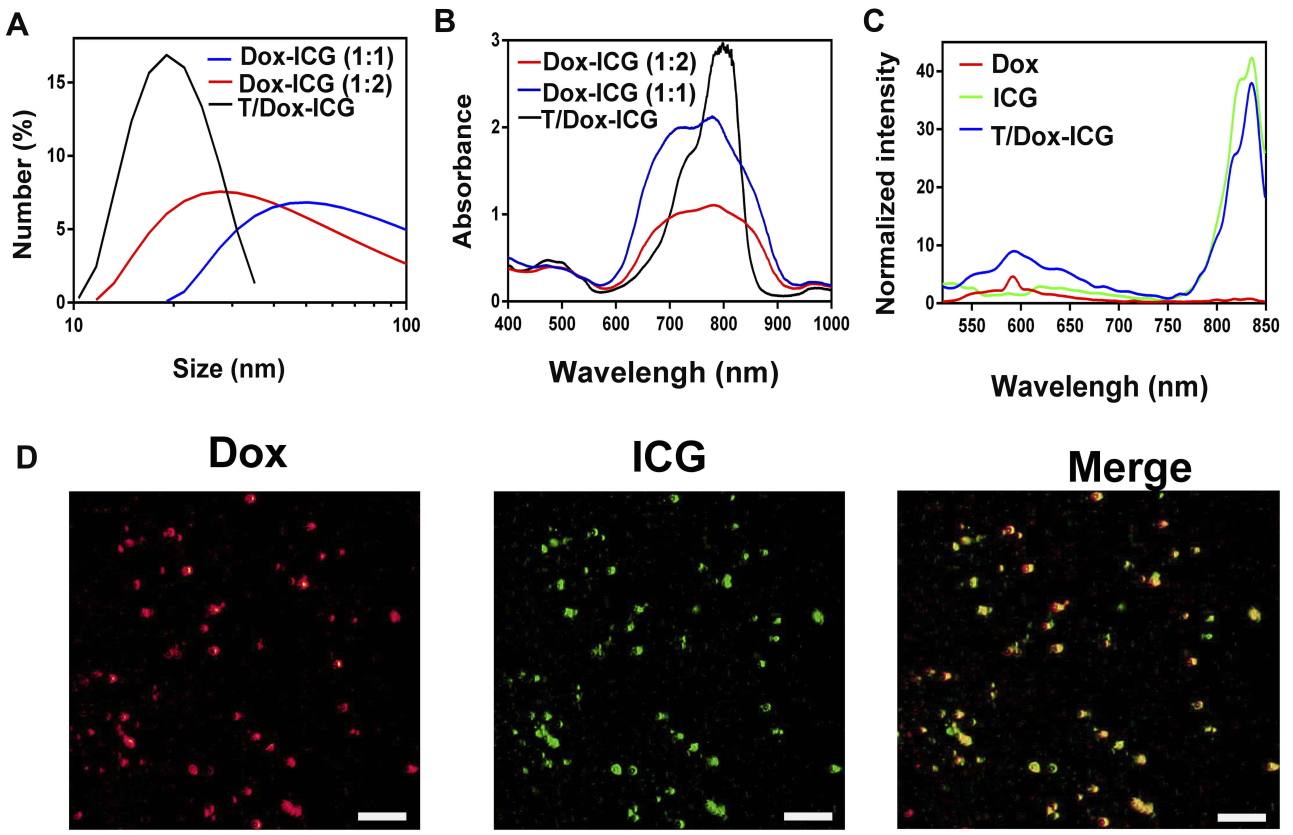

Figure 3 (**A**) DLS of the Dox-ICG (1:2), Dox-ICG (1:1) and T/Dox-ICG NPs (1:1:1). (**B**) Absorbance spectra of Dox-ICG (1:2), Dox-ICG (1:1) and T/Dox-ICG NPs (1:1:1) aqueous solutions. (**C**) The fluorescence spectra of free Dox, free ICG and T/Dox-ICG NPs. (**D**) CLSM images of Dox and ICG, red means Dox, green means ICG, yellow means the merge of Dox and ICG (Scale bar, 100 nm).

because a large proportion of the two drugs was not adequately nanosized. In addition, the zeta potential of Dox-ICG NPs increased from approximately −30 mV to −20.1 mV by adjusting the mass ratio of Dox to ICG (Figure S1), suggesting there was electrostatic interactions between Dox and ICG. The emergence of multidrug resistance (MDR) remains a major hurdle in cancer chemotherapy. Various strategies including MDR modulators, multifunctional nanocarriers, and RNAi therapy, have been conducted to overcome these MDR mechanisms. The main drawback of MDR modulators is the unacceptably high toxicity that subsequently limited their clinical trials.[14] Meanwhile, multifunctional nanocarriers and RNA interference (RNAi) therapy require a sophisticated DDS design, therefore, their application also yielded generally disappointing results. TPGS is an FDA-approved excellent emulsifier as well as drug stabilizer, and is utilized to reverse MDR. Therefore, we designed a self-assembly nanoplatform modified with TPGS. After the TPGS was added, TEM showed that the T/Dox-ICG NPs showed good monodispersity (Figure 2C), scanning electron microscopy (SEM) images also revealed the diameter of T/Dox-ICG NPs (Figure 2D). DLS showed its average diameter is about 19.03 nm, which was smaller than ICG-Dox, the results of DLS also confirmed their size distributions displayed a cramped feature, which means T/Dox-ICG NPs were more dispersed (Figure 3A). The UV-vis-NIR of the T/ICG-Dox NPs was compared to that of the ICG-Dox, and the value at 808 nm of T/ICG-Dox NPs was the highest, which for the further photothermal property study under the 808 nm laser (Figure 3B). The fluorescence spectra of Dox, ICG and T/Dox-ICG NPs are shown in Figure 3C. Confocal laser scanning microscopy (CLSM) images showed that both Dox (red color) and ICG (green color) dyes were distributed throughout the co-self-assembly NPs, and the yellow color indicated the merge of Dox and ICG (Figure 3D). More importantly, the content of Dox and ICG was measured to be ~32.56 wt% and ~25.67wt% (encapsulation efficiency of Dox and ICG was tested to be ~95.3% and ~92.4%), respectively. What's more, there is was no precipitation after incubation in water, PBS, NaCl, DMEM or FBS, suggesting that T/Dox-ICG NPs are stable and can be stored without sedimentation or aggregation (Figure S2). This revealed the T/ICG-Dox NPs were steadfast.

In vitro FL Imaging

Because T/Dox-ICG NPs had strong NIR absorbance, we then tested and quantified their FL property. As expected, the T/Dox-ICG NPs showed more notable FL signal than Dox-ICG and free ICG (Figure 4A and B). An enhanced FL signals likely suggests that a greater concentration of ICG in self-assembly NPs. These results confirmed T/Dox-ICG NPs have a good potential for imaging-guided therapy.

In vitro Photothermal Effect

To investigate the photothermal conversion efficiency of T/Dox-ICG NPs. In our experiment, the temperature changes of free ICG, Dox-ICG, and T/Dox-ICG NPs solutions upon NIR laser irradiation (808 nm, 1 W/cm^2) were evaluated at different times. As shown in Figure 4C and D, as the irradiation time increased, the temperatures of T/Dox-ICG NPs increased accordingly. After 5 min laser irradiation, the temperature of free ICG, Dox-ICG, and T/Dox-ICG NPs reached 39.82, 43.83 and 56.96°C, respectively, indicating that free ICG has poor photostability. In addition, the Dox-ICG showed a higher temperature than free ICG, which suggests a higher concentration of ICG within Dox-ICG was formed by Dox and ICG. The results demonstrated the enhanced PTT effect of T/Dox-ICG NPs.

In vitro Dox and ICG Release

In vitro Dox and ICG release profiles were evaluated by dialysis in PBS at pH 7.4, and 5.4 at 37°C, respectively. As the results in Figure 5, the releasing of T/Dox-ICG NPs was based on different pH conditions. Both Dox and ICG showed burst release at first both in the normal physiological pH (pH 7.4) and acidic condition (pH 5.4). However, it was followed by a controlled releasing phase, in which the Dox and ICG showed a slow release at pH 7.4 after 12 h, and only about 36.87% of Dox and 39.65% of ICG were released over 24 h. Nevertheless, in the next 48 h, the cumulative release of Dox and ICG was increased to 88.76% and 79.83% at acidic pH 5.4, respectively. The result could be ascribed to the

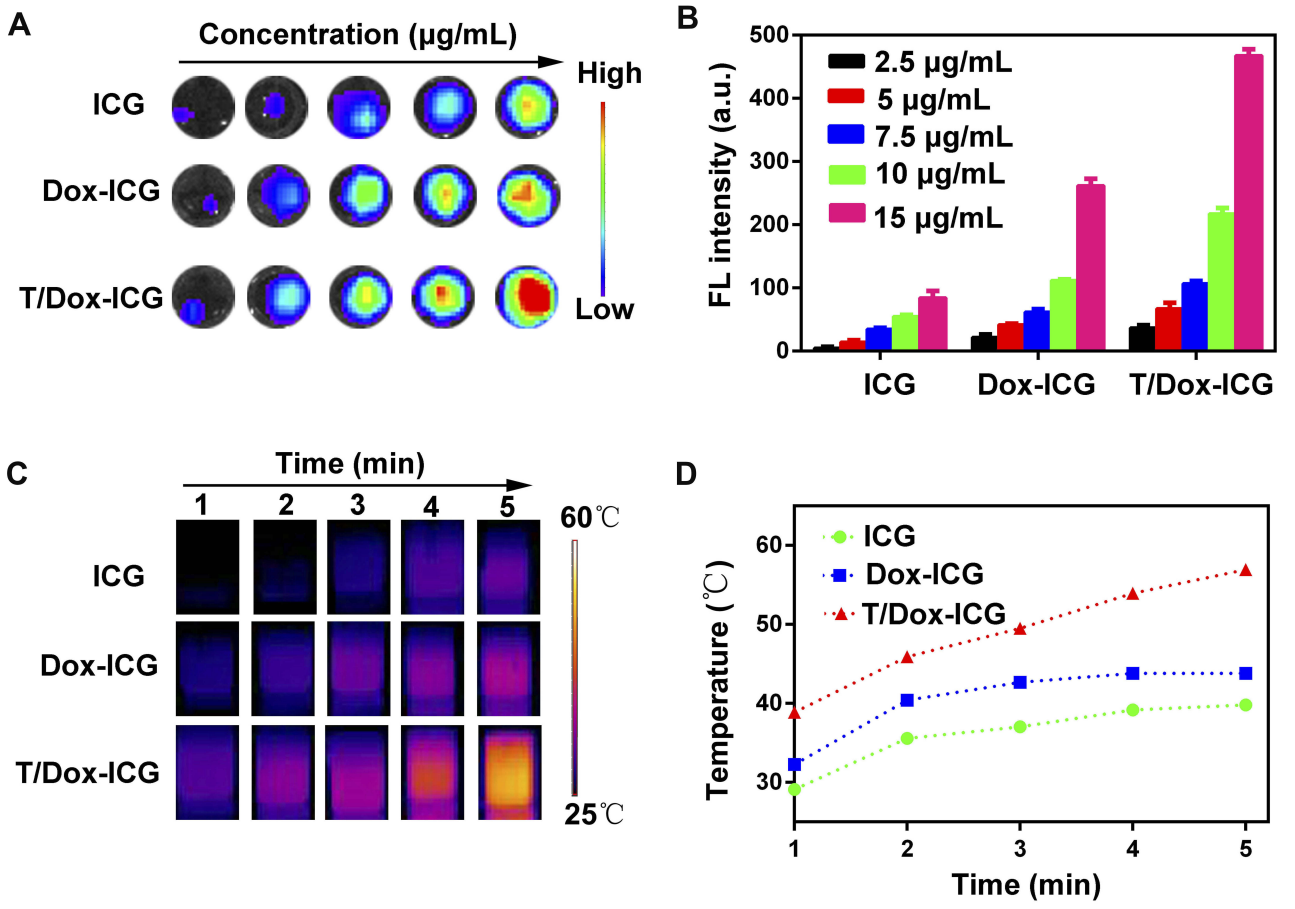

Figure 4 (**A**) FL images and (**B**) FL signal intensity of free ICG, Dox-ICG and T/Dox-ICG NPs with different ICG concentrations. (**C**) Infrared thermographic images and (**D**) photothermal heating curves of free ICG, Dox-ICG and T/Dox-ICG NPs under 808 nm laser irradiation (1 W/cm^2, 5 min).

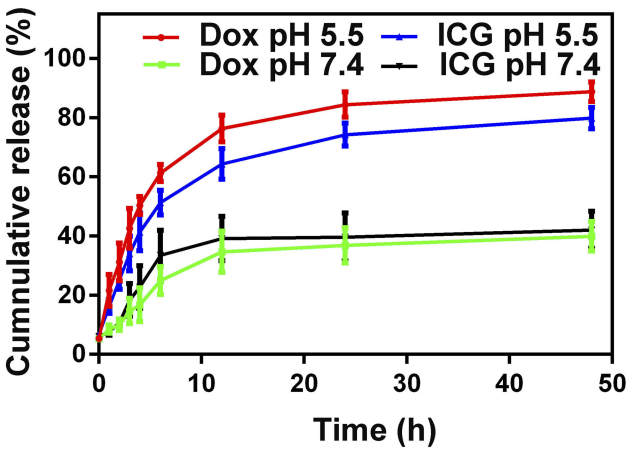

Figure 5 Cumulative release of Dox and ICG from T/Dox-ICG NPs at pH 7.4 and 5.5.

protonation of Dox in an acidic environment, thus the hydrophobic interaction between Dox and ICG was weakened. The results revealed T/Dox-ICG NPs might have lower toxicity in normal tissue during anticancer treatment.

Western-Blot Assay

The MDR occurs mainly include overexpressed MDR protein P-gp, which can reduce intracellular drug concentration and mediate MDR. TPGS has been found to inhibit P-gp and reverse MDR. A Western blot assay was performed to analyze P-gp expression levels in SCG7901/VCR cells after incubation with T/Dox-ICG NPs (Figure 6A). The control and Dox-ICG showed no obvious inhibition of P-gp expression. However, it was found that T/Dox-ICG NPs exhibited significant inhibition of P-gp expression. The relevant P-gp expression was calculated by the signal intensity of the protein bands (Figure 6B). The results suggest that the effective cytotoxicity activity of T/Dox-ICG NPs maybe attributed to TPGS-mediated P-gp inhibition.

In vitro Cellular Uptake and Intracellular Distribution of Dox

To investigate the cellular internalization of Dox, SCG 7901/VCR cells were incubated with Dox-ICG and T/Dox-ICG NPs and then assessed by CLSM. As shown in Figure 7A, at 12 h, the cellular uptake of Dox-ICG group, the red fluorescence of Dox was mainly localized in cytoplasm, whereas T/Dox-ICG NPs were transported into nucleus at the same time. It should be noted that after 24 h, the red fluorescence of Dox moved into the nucleus in the SCG 7901/VCR cells. The qualitative result of Image J analysis confirmed a significant amount of Dox in the nucleus of the SCG 7901/VCR cells (Figure 7B). Meanwhile, free DOX was efficiently exported by overexpressing P-gp; thus, the amount of intracellular DOX was rapidly eliminated (Figure S3). This means without TPGS, the entry of Dox into the nucleus was inhibited in SCG 7901/VCR cells, but with the aid of TPGS, the enrichment of Dox inside the nucleus was facilitated. Along this line of thinking, TPGS might affect mitochondrial structure and function, thereby reversing tumor resistance.

In vitro Chemotherapy, PTT, and Chemo-PTT Treatments

The cytotoxicity of different materials against SCG 7901/VCR cells was evaluated by the MTT assay. SCG 7901/VCR cells were incubated with ICG, ICG +laser (808 nm laser irradiation 1W/cm^2, 5 min), Dox, Dox-ICG, T/Dox-ICG NPs, T/Dox-ICG NPs +laser (808 nm laser irradiation,1W/cm^2, 5 min), respectively. The T/Dox-ICG NPs +laser group showed much more cytotoxicity with the cell killing efficacy was reach to ~91.25%. And with free ICG, the cells showed greater survival

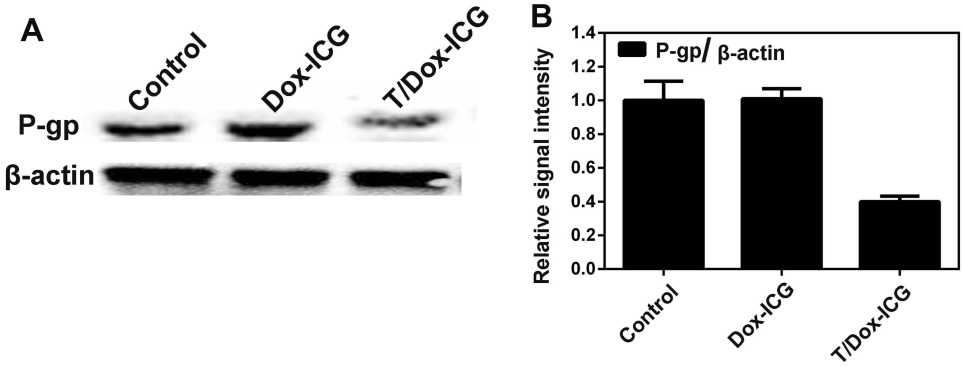

Figure 6 (**A**) Detection of P-gp knockdown in SCG7901/VCR cells by T/Dox-ICG using Western blot and (**B**) the relevant P-gp expression was calculated by the signal intensity of the protein bands.

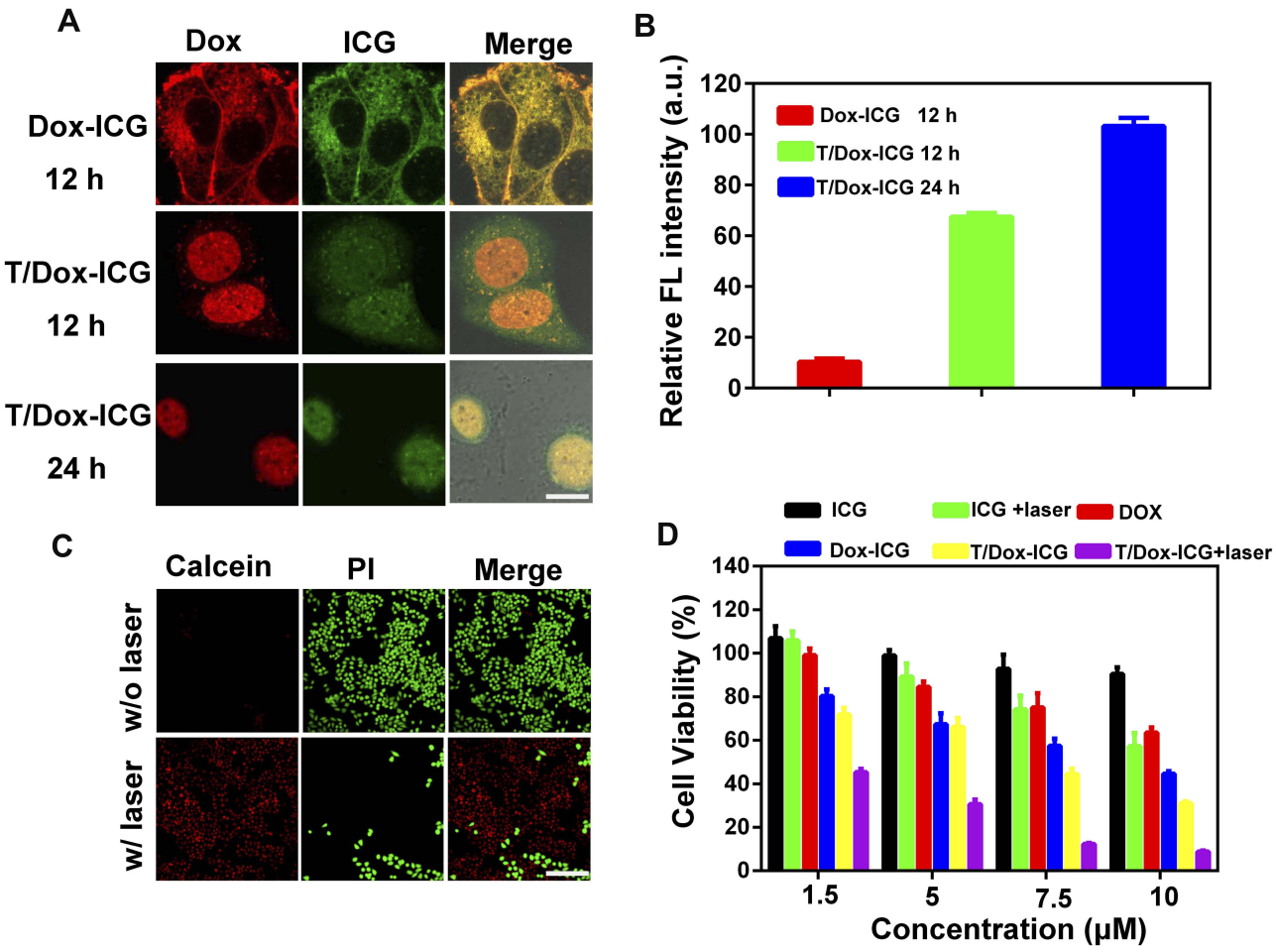

Figure 7 (**A**) CLAM of Dox-ICG and T/Dox-ICG NPs incubation with SCG7901/VCR cells for different times (Scale bar, 50 μm). Merged images display the overlay of red autofluorescence of Dox and green fluorescence of ICG. (**B**) Nuclear uptake of DOX bySCG7901/VCR cells. (**C**) Fluorescence images of calcein AM/PI stained SCG7901/VCR cells after T/Dox-ICG NPs treatments with or without laser irradiation (Scale bar, 20 μm). (**D**) Cell viability of SCG7901/VCR cells after various treatments for 24 h.

rate. The T/Dox-ICG NPs group showed higher cytotoxicity than free Dox and Dox-ICG, which could be interpreted by an enhanced cellular uptake, and cells are more sensitive to Dox after TPGS inhibited the expression of P-gp (Figure 7D). This result was also examined by the co-staining assay. Cells were stained with calcein-AM and PI, in which dead cells were stained by PI (red fluorescence) and live cells were stained by calcein-AM (green fluorescence). In the control, there was no red fluorescence, but the T/Dox-ICG NPs +laser treated cells showed significant difference with red fluorescence signals (Figure 7C). All the results revealed that T/Dox-ICG NPs NPs had enhanced effect in Dox delivery and chemo-PTT treatment.

Conclusion

In summary, we successfully synthesized a novel multifunctional T/Dox-ICG NPs for imaging-guided chemo-PTT combination therapy and overcome MDR. T/Dox-ICG NPs displayed ample stability in water, good monodispersity, higher drug-loading efficiency and excellent drug-releasing profile in tumor environment. T/Dox-ICG NPs showed enhanced FL imaging and high photothermal conversion properties. The FL intensity of T/Dox-ICG NPs was 5.53 times and the temperature of T/Dox-ICG NPs was 17.14°C higher than free ICG. Compared with Dox-ICG, the T/Dox-ICG NPs exhibited more significant nuclear localization of Dox in SCG7901/MDR cells, as TPGS had an evident effect on the inhibition of P-gp. T/Dox-ICG NPs with laser can induce higher cytotoxicity on MDR cells compared with other groups, its cell survival was only 8.75%. Taken together, T/Dox-ICG NPs provide a promising carrier for imaging-guided combination therapy, and further overcome P-gp mediated MDR to improve anticancer effect.

Acknowledgments

This research was supported by the National Key R&D Program of China (2017YFE0103600), National Natural Science Foundation of China (81720108021, 81772009, 81601466), Scientific and Technological Research Project of Henan Province (182102310162) and Zhongyuan Thousand Talents Plan Project– Basic Research Leader Talent (ZYQ R201810117).

Disclosure

The authors report no conflicts of interest in this work.

References

1. Siegel R, Miller KD, Jemal A. Cancer statistics. 2017. *CA Cancer J Clin*. 2017;67(1):7–30. doi:10.3322/caac.21387
2. Nomura H. Safe Handling of Cancer Chemotherapy Drugs in Pharmacy (Preparations, Transport and Safe Deposit). Cancer & Chemotherapy. 2017;44(7):554–557.
3. Jia Y, Wang X, Hu D, et al. Phototheranostics: active targeting of orthotopic glioma using biomimetic proteolipid nanoparticles. *ACS Nano*. 2019;13(1):386–398. doi:10.1021/acsnano.8b06556
4. Blanco E, Shen H, Ferrari M. Principles of nanoparticle design for overcoming biological barriers to drug delivery. *Nat Biotechnol*. 2015;33(9):941–951. doi:10.1038/nbt.3330
5. Zhang R, Cheng K, Antaris AL, et al. Hybrid anisotropic nanostructures for dual-modal cancer imaging and image-guided chemo-thermo therapies. *Biomaterials*. 2016;103:265–277. doi:10.1016/j.biomaterials.2016.06.063
6. Bayat Mokhtari R, Homayouni TS, Baluch N, et al. Combination therapy in combating cancer. *Oncotarget*. 2017;8(23):38022–38043. doi:10.18632/oncotarget.16723
7. Zhang J, Liang YC, Lin X, et al. Self-monitoring and self-delivery of photosensitizer-doped nanoparticles for highly effective combination cancer therapy in vitro and in vivo. *ACS Nano*. 2015;9(10):9741–9756. doi:10.1021/acsnano.5b02513
8. Hou W, Zhao X, Qian X, et al. pH-Sensitive self-assembling nanoparticles for tumor near-infrared fluorescence imaging and chemo-photodynamic combination therapy. *Nanoscale*. 2016;8(1):104–116. doi:10.1039/C5NR06842H
9. Wu G, Fan X, Li L, et al. Interaction of antimicrobial peptide s-thanatin with lipopolysaccharide in vitro and in an experimental mouse model of septic shock caused by a multidrug-resistant clinical isolate of Escherichia coli. *Int J Antimicrob Agents*. 2010;35(3):250–254. doi:10.1016/j.ijantimicag.2009.11.009
10. Zheng T, Wang W, Wu F, et al. Zwitterionic polymer-gated Au@TiO2 core-shell nanoparticles for imaging-guided combined cancer therapy. *Theranostics*. 2019;9(17):5035–5048.
11. Wang X, Cheng L. Multifunctional two-dimensional nanocomposites for photothermal-based combined cancer therapy. *Nanoscale*. 2019;11:15685–15708.
12. Li Y, Liu G, Ma J, et al. Chemotherapeutic drug-photothermal agent co-self-assembling nanoparticles for near-infrared fluorescence and photoacoustic dual-modal imaging-guided chemo-photothermal synergistic therapy. *J Control Release*. 2017;258:95–107. doi:10.1016/j.jconrel.2017.05.011
13. Song XR, Cai Z, Zheng Y, et al. Reversion of multidrug resistance by co-encapsulation of vincristine and verapamil in PLGA nanoparticles. *Eur J Pharm Sci*. 2009;37(3–4):300–305. doi:10.1016/j.ejps.2009.02.018
14. Shukla S, Wu CP, Ambudkar SV. Development of inhibitors of ATP-binding cassette drug transporters: present status and challenges. *Expert Opin Drug Metab Toxicol*. 2008;4(2):205–223. doi:10.1517/17425255.4.2.205
15. Xu C, Wang P, Zhang J, et al. Pulmonary codelivery of doxorubicin and siRNA by pH-sensitive nanoparticles for therapy of metastatic lung cancer. *Small*. 2015;11(34):4321–4333. doi:10.1002/smll.201501034
16. Akinc A, Zumbuehl A, Goldberg M, et al. A combinatorial library of lipid-like materials for delivery of RNAi therapeutics. *Nat Biotechnol*. 2008;26(5):561–569. doi:10.1038/nbt1402
17. Meng H, Mai WX, Zhang H, et al. Codelivery of an optimal drug/siRNA combination using mesoporous silica nanoparticles to overcome drug resistance in breast cancer in vitro and in vivo. *ACS Nano*. 2013;7(2):994–1005. doi:10.1021/nn3044066
18. Li D, Gale RP, Liu Y, et al. 5′-Triphosphate siRNA targeting MDR1 reverses multi-drug resistance and activates RIG-I-induced immune-stimulatory and apoptotic effects against human myeloid leukaemia cells. *Leuk Res*. 2017;58:23–30. doi:10.1016/j.leukres.2017.03.010
19. Lin G, Zhu W, Yang L, et al. Delivery of siRNA by MRI-visible nanovehicles to overcome drug resistance in MCF-7/ADR human breast cancer cells. *Biomaterials*. 2014;35(35):9495–9507. doi:10.1016/j.biomaterials.2014.07.049
20. Li Z, Liu J, Hu Y, et al. Multimodal imaging-guided antitumor photothermal therapy and drug delivery using bismuth selenide spherical sponge. *ACS Nano*. 2016;10(10):9646–9658. doi:10.1021/acsnano.6b05427
21. Wang J, Guo F, Yu M, et al. Rapamycin/DiR loaded lipid-polyaniline nanoparticles for dual-modal imaging guided enhanced photothermal and antiangiogenic combination therapy. *J Control Release*. 2016;237:23–34. doi:10.1016/j.jconrel.2016.07.005
22. Li S, Sun Z, Deng G, et al. Dual-modal imaging-guided highly efficient photothermal therapy using heptamethine cyanine-conjugated hyaluronic acid micelles. *Biomater Sci*. 2017;5(6):1122–1129. doi:10.1039/C7BM00230K
23. Sun Q, You Q, Pang X, et al. A photoresponsive and rod-shape nanocarrier: single wavelength of light triggered photothermal and photodynamic therapy based on AuNRs-capped & Ce6-doped mesoporous silica nanorods. *Biomaterials*. 2017;122:188–200. doi:10.1016/j.biomaterials.2017.01.021
24. Sun S, Chen J, Jiang K, et al. Ce6-modified carbon dots for multimodal-imaging-guided and single-NIR-laser-triggered photothermal/photodynamic synergistic cancer therapy by reduced irradiation power. *ACS Appl Mater Interfaces*. 2019;11(6):5791–5803. doi:10.1021/acsami.8b19042
25. Hu S, Lee E, Wang C, et al. Amphiphilic drugs as surfactants to fabricate excipient-free stable nanodispersions of hydrophobic drugs for cancer chemotherapy. *J Control Release*. 2015;220(Pt A):175–179. doi:10.1016/j.jconrel.2015.10.031
26. Baba K, Pudavar HE, Roy I, et al. New method for delivering a hydrophobic drug for photodynamic therapy using pure nanocrystal form of the drug. *Mol Pharm*. 2007;4(2):289–297. doi:10.1021/mp060117f
27. Huang P, Wang D, Su Y, et al. Combination of small molecule prodrug and nanodrug delivery: amphiphilic drug-drug conjugate for cancer therapy. *J Am Chem Soc*. 2014;136(33):11748–11756. doi:10.1021/ja505212y
28. Pei Q, Hu X, Liu S, et al. Paclitaxel dimers assembling nanomedicines for treatment of cervix carcinoma. *J Control Release*. 2017;254:23–33. doi:10.1016/j.jconrel.2017.03.391
29. Bisht S, Maitra A. Dextran-doxorubicin/chitosan nanoparticles for solid tumor therapy. *Wiley Interdiscip Rev Nanomed Nanobiotechnol*. 2009;1(4):415–425. doi:10.1002/wnan.43
30. Mou Q, Ma Y, Zhu X, et al. A small molecule nanodrug consisting of amphiphilic targeting ligand-chemotherapy drug conjugate for targeted cancer therapy. *J Control Release*. 2016;230:34–44. doi:10.1016/j.jconrel.2016.03.037

31. Ejima H, Richardson JJ, Liang K, et al. One-step assembly of coordination complexes for versatile film and particle engineering. *Science*. 2013;341(6142):154–157. doi:10.1126/science.1237265
32. Kim S, Kwak S, Lee S, et al. One-step functionalization of zwitterionic poly[(3-(methacryloylamino)propyl)dimethyl(3-sulfopropyl)ammonium hydroxide] surfaces by metal-polyphenol coating. *Chem Commun (Camb)*. 2015;51(25):5340–5342. doi:10.1039/C4CC08609K
33. Su H, Zhang P, Cheetham AG, et al. Supramolecular crafting of self-assembling camptothecin prodrugs with enhanced efficacy against primary cancer cells. *Theranostics*. 2016;6(7):1065–1074. doi:10.7150/thno.15420
34. Ma W, Su H, Cheetham AG, et al. Synergistic antitumor activity of a self-assembling camptothecin and capecitabine hybrid prodrug for improved efficacy. *J Control Release*. 2017;263:102–111. doi:10.1016/j.jconrel.2017.01.015
35. Cagel M, Grotz E, Bernabeu E, et al. Doxorubicin: nanotechnological overviews from bench to bedside. *Drug Discov Today*. 2017;22(2):270–281. doi:10.1016/j.drudis.2016.11.005
36. Wu Y, Zhang Y, Zhang W, et al. Reversing of multidrug resistance breast cancer by co-delivery of P-gp siRNA and doxorubicin via folic acid-modified core-shell nanomicelles. *Colloids Surf B Biointerfaces*. 2016;138:60–69. doi:10.1016/j.colsurfb.2015.11.041
37. Cai W, Gao H, Chu C, et al. Engineering phototheranostic nanoscale metal-organic frameworks for multimodal imaging-guided cancer therapy. *ACS Appl Mater Interfaces*. 2017;9(3):2040–2051. doi:10.1021/acsami.6b11579
38. Zhang Z, Tan S, Feng SS. Vitamin E TPGS as a molecular biomaterial for drug delivery. *Biomaterials*. 2012;33(19):4889–4906. doi:10.1016/j.biomaterials.2012.03.046
39. Guo Y, Luo J, Tan S, et al. The applications of Vitamin E TPGS in drug delivery. *Eur J Pharm Sci*. 2013;49(2):175–186. doi:10.1016/j.ejps.2013.02.006
40. Yang C, Wu T, Qi Y, et al. Recent advances in the application of Vitamin E TPGS for drug delivery. *Theranostics*. 2018;8(2):464–485. doi:10.7150/thno.22711
41. Zhang Z, Feng SS. The drug encapsulation efficiency, in vitro drug release, cellular uptake and cytotoxicity of paclitaxel-loaded poly(lactide)-tocopheryl polyethylene glycol succinate nanoparticles. *Biomaterials*. 2006;27(21):4025–4033. doi:10.1016/j.biomaterials.2006.03.006
42. Kulkarni SA, Feng SS. Effects of particle size and surface modification on cellular uptake and biodistribution of polymeric nanoparticles for drug delivery. *Pharm Res*. 2013;30(10):2512–2522. doi:10.1007/s11095-012-0958-3
43. Shieh MJ, Hsu CY, Huang LY, et al. Reversal of doxorubicin-resistance by multifunctional nanoparticles in MCF-7/ADR cells. *J Control Release*. 2011;152(3):418–425. doi:10.1016/j.jconrel.2011.03.017
44. Hao T, Chen D, Liu K, et al. Micelles of d-alpha-Tocopheryl Polyethylene Glycol 2000 Succinate (TPGS 2K) for doxorubicin delivery with reversal of multidrug resistance. *ACS Appl Mater Interfaces*. 2015;7(32):18064–18075. doi:10.1021/acsami.5b04995
45. Wang DF, Rong WT, Lu Y, et al. TPGS2k/PLGA nanoparticles for overcoming multidrug resistance by interfering mitochondria of human alveolar adenocarcinoma cells. *ACS Appl Mater Interfaces*. 2015;7(7):3888–3901. doi:10.1021/am508340m